Energy Geostructures for Reducing Energy Consumption in Hong Kong: An Example of Energy Diaphragm Wall

Leung, A. K.[1*], Wang, Y. H.[1], Yang, H. X.[2], Zhou, H.[2], and Zhou, C.[3]
[1]*Department of Civil and Environmental Engineering, The Hong Kong University of Science and Technology, Hong Kong SAR, China*
[2]*Department of Building Environment and Energy Engineering, The Hong Kong Polytechnic University, Hong Kong SAR, China*
[3]*Department of Civil and Environmental Engineering, The Hong Kong Polytechnic University, Hong Kong SAR, China*
*Corresponding author: ceanthony@ust.hk

doi: https://doi.org/10.21467/proceedings.171.12

ABSTRACT

Energy geostructure is a green construction technology that turns geostructures such as piles, walls and tunnels to underground heat exchangers; by embedding polyethylene pipes in the concrete body of these geostructures, they could be used to inject heat into the ground in summer for space cooling and extract heat from the ground in winter for space heating, through the control of ground-source heat pump (GSHP). By exchanging ground energy, energy geostructures represent an advantageous technology to reduce energy consumption of air-conditioning nearby buildings sustainably. However, adoption of this technology in Hong Kong is slow primarily because of high cooling load and declining energy efficiency caused by ground thermal imbalances. This study presents a series of finite-element simulations to demonstrate the energy and structural performance of hypothetical, GSHP-coupled, reinforced concrete energy diaphragm wall panels, when operated under long-term extreme and realistic energy use scenarios in Hong Kong for an underground shopping mall. Changes in heat exchange efficiency due to continuous heat injection to the ground are presented. Implications in the engineering design of the diaphragm wall due to the additional thermal functioning through detailed analysis of soil-structure interaction are discussed.

1. INTRODUCTION

In the next decades, vast infrastructure development is needed to support the Hong Kong (HK) Government's '*Hong Kong 2030+*' spatial development strategy, which includes mega projects such as *Lantau Tomorrow Vision* and *Northern Metropolis development strategy*. Underground construction is indispensable to the success and sustainability of all these development plans, but it is also one of the major contributors to carbon emissions. In 2021, about 90% of energy consumption (159,100 TJ) in HK was electricity (EMSD, 2022), more than 30% of which had been used for air conditioning in both residential and commercial sectors. Electricity generation constitutes more than 60% of greenhouse gas emissions in the year. Due to the impending urbanisation plans, future energy demand is expected to increase. It is thus vital to develop green construction technologies that can effectively reduce the energy consumption of infrastructures, especially for air-conditioning.

Energy geostructures are innovative, green construction technologies, by transforming geostructures such as piles, tunnels and diaphragm walls into underground heat exchangers (Fig. 1). The concrete body of these geostructures are embedded with high-density polyethylene (HDPE) pipes. Through ground-source heat pumps (GSHPs), the energy geostructures can inject heat into the ground (heat sink) in summer for space cooling and extract heat from the ground (heat source) in winter for space heating. By exchanging ground energy, energy geostructures represent an advantageous technology to meet the energy requirements of nearby buildings sustainably, helping Hong Kong to accomplish '*net-zero carbon emission for electricity generation*'.

This kind of construction technology has been used in Europe, the UK and North America, and the energy efficiency and structural and geotechnical behaviour of energy geostructures in different forms (especially piles)

Proceedings DOI: 10.21467/proceedings.171; Series: AIJR Proceedings; ISSN: 2582-3922; ISBN: 978-81-970666-7-2

when operated in these regions have been investigated. However, the uptake of this technology in Hong Kong and other cities located in the tropical to subtropical regions is slow. This is primarily because the cooling load dominates the energy demands in these regions, and the heat transfer efficiency between energy geostructures and the surrounding soil is *thought* to be low as the efficiency reduces with time due to the thermal imbalance issues in the ground under long-term GSHP operation. How the additional thermal functionality may affect the soil–structure interaction and the structural performance of the energy geostructures, especially when operated under the Hong Kong environment, is unknown.

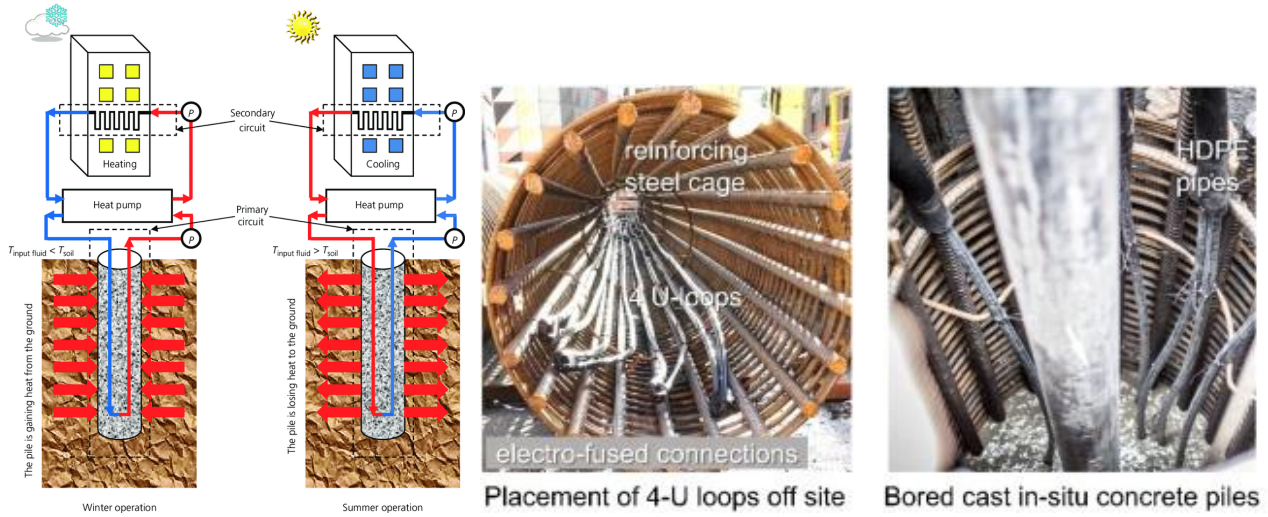

(a) (b)

Figure 1: (a) Schematic of GSHP-coupled energy pile system (after Abuel-Nage et al., 2013); and (b) two images showing the U-shaped HDPE pipe loop attached on the reinforcement cage of a RC bored pile (after Zhong et al. 2022).

The objective of this study is to investigate the potential of the application of energy geostructure in the form of diaphragm wall (i.e. energy wall) in Hong Kong. A series of finite-element (FE) simulations was carried out to determine the energy and structural performance of hypothetical, GSHP-coupled, reinforced concrete (RC) energy wall panels when operated under extreme and realistic energy consumption scenarios in Hong Kong for an underground shopping mall. Through FE thermal analysis which took into account the heat-and-mass transport process in the soil-wall system, temporal variations of the coefficient of performance (COP) of long-term GSHP operation were determined to aid the evaluation of the significance of performance degradation and energy consumption over time due to thermal imbalance. FE soil–structure thermomechanical interaction analysis was also conducted to determine the wall responses during staged excavation and the subsequent GSHP operation stage. Any additional wall movement and bending due to the thermal functioning were evaluated.

2 METHODOLOGY

2.1 Hypothetical case study and modelling approach

The deep excavation work of the Dragon Centre, Hong Kong, presented by Lui & Yau (1995), was selected as the reference case study for the analysis in this study. The plane area of excavation was 107 m × 67 m and the excavation depth was 27 m. The work adopted the top-down construction method, and the excavation and lateral system (ELS) included multiple panels of 50 m-deep reinforced concrete (RC) diaphragm wall propped with five levels of RC slabs. Each wall panel has a width of 1.2 m, a length of 2.14 m and a depth of 50 m. In this study, the diaphragm wall along the long side of the excavation was hypothetically considered as the energy wall, i.e. with a heat exchange function by integrating a U-shaped heat exchange loop in each wall panel.

Energy efficiency and structural responses of the energy walls due to thermomechanical soil–structure interaction were analysed. Two types of analysis were conducted. The first analysis focused on heat-and-mass transport processes, with an aim to assess the COP (i.e. a measure of energy efficiency of the whole system). The second analysis focused on the thermomechanical behaviour of the energy wall when subjected to thermal loadings during the operation phase, aiming to determine additional mechanical stress and strain introduced by the thermal function.

Proceedings DOI: 10.21467/proceedings.171
ISBN: 978-81-970666-7-2

Series: AIJR Proceedings
ISSN: 2582-3922

2.2 Thermal analysis

The three-dimensional (3-D) FE platform, COMSOL Multiphysics (version 6.2), was used to evaluate the heat transfer processes within the soil–energy wall system and the heat transfer efficiency of the energy wall. Detailed model setup, boundary and initial conditions, governing equations, input parameters and analysis plan are explained in the following sections.

2.2.1 Model setup, initial conditions and boundary conditions

Figures 2(a) and (b) show a 3-D and cross-section view of the FE mesh of the deep excavation. Due to symmetry, only half of the excavation was modelled, totaling 506,116 elements. Following the site investigation reported by Lui & Yau (1995), four uniform soil layers were considered in the model, comprising of a 5 m-thick loose fill layer overlain a 5 m-thick loose marine deposit (MD) layer, a 30.5 m-thick dense to very dense completely decomposed granite (CDG) layer and finally a 50 m-thick moderate decomposed granite (MDG) stratum. The diaphragm wall along the long-side of the excavation (i.e. 107 m) were hypothetically modified to be the energy wall, whereas those along the short side were non-thermal walls. The energy wall was composed of 50 wall panels that were thermomechanically connected, each of which has a cross-section area of 2.14 m (length) × 1.2 m (thick). In each panel, a single U-shaped heat exchange loop was embedded and modelled (Fig. 2(a)). The distance between the inlet and outlet tubes (both with an inner diameter of 25 mm) was 1 m. The presence of a U-shaped loop in each wall panel meant a reduction of cross-section area of 1.5×10^{-5}%. Pipe flow was modelled in the loop to simulate the heat transfer process. The flow rate of the circulating fluid (i.e. water, in

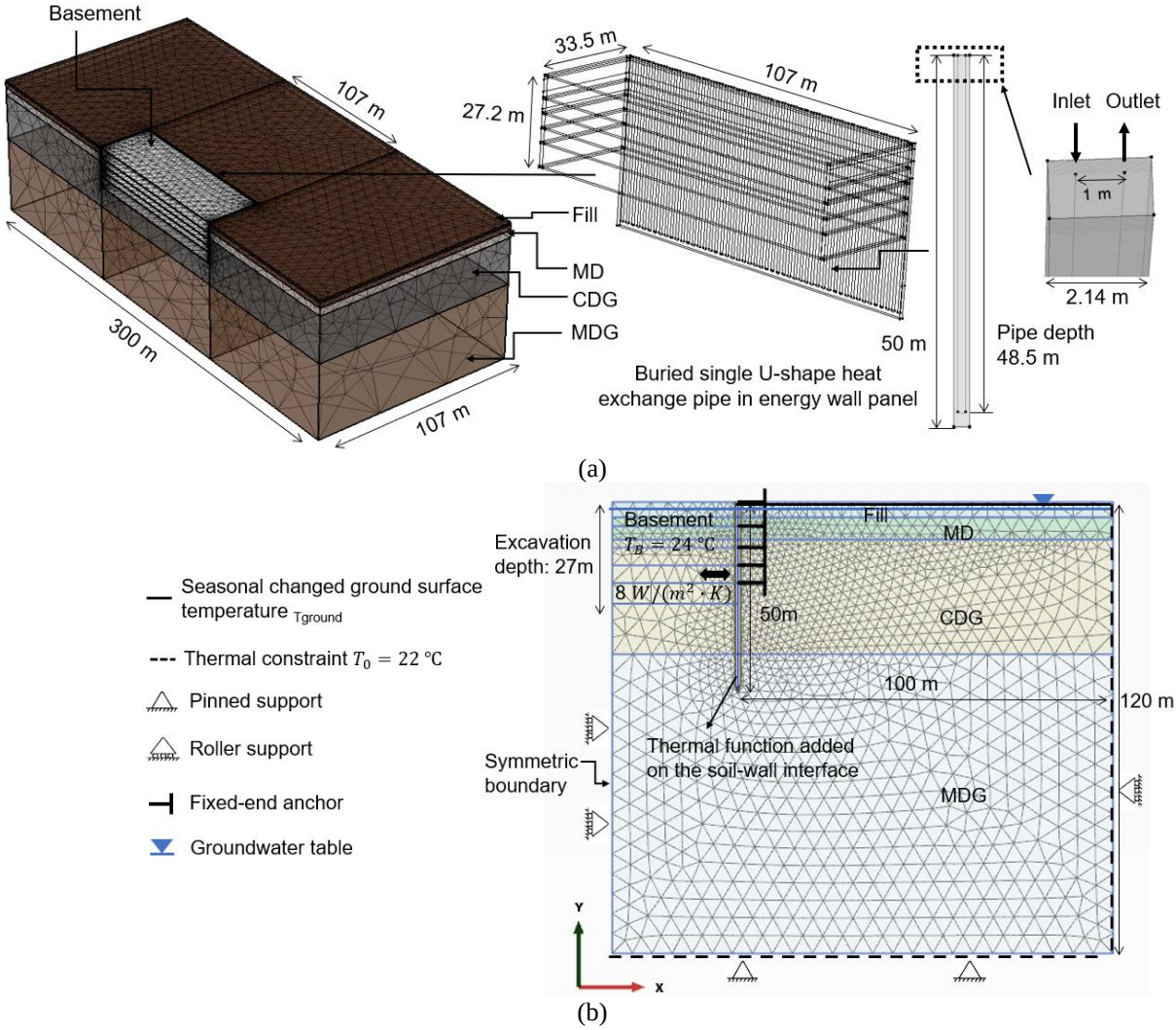

Figure 2: Numerical model geometry and FE mesh; (a) 3D layout of the COMSOL model; (b) section view of the PLAXIS model.

this case) was set to 0.25 m/s, which was sufficient to generate turbulent flow within the U-shaped pipes required for efficient heat exchange (Ground Source Heat Pump Association, 2012). The lateral support system consisted of five levels of identical 450 mm-thick RC slabs (except the bottommost slab that was 700 mm thick) located at 6.4, 12.1, 16.8, 21.5 and 27.2 m below the ground surface, forming a basement.

All the non-thermal and thermal wall panels were modelled by solid elements, whilst the surrounding soils were modelled by porous media. The heat transfer between the circulating fluid of the U-shaped pipes (i.e. water) and the pipe wall was modelled through the dimensionless Nusselt number (Nu), which describes the relative importance between the convective to conductive heat transfer rate within fluid flow. In this study, Nu was set to be 3.66 for heat transfer in fully developed turbulent pipe flow based on the Dittus-Boelter correlation.

Based on the borehole survey conducted by Cui et al. (2008), the underground temperature in Hong Kong was approximately constant at 22 °C at depths below 10 m, which was thus set as the initial ground temperature uniformly for all soil layers and remained constant at the far sides and bottom boundaries of the model. A 25-year seasonal variation in ground surface temperature with time was applied, according to an equation model validated against the observation records at two meteorological stations: (i) the Hong Kong Observatory Headquarters (HKO) from 1996-2005 and (ii) the King's Park Meteorological Station (KP) from 2008-2009 ((Chow et al., 2011). The ground surface temperature was considered to vary between 18.7 and 29.9 °C annually following a sinusoidal pattern and this pattern was repeated for 25 times. On the symmetrical side, the adiabatic boundary was imposed. For other sides, the Dirichlet's boundary condition was applied. Moreover, the indoor temperature of the basement was set as a constant value of 24°C, which is the desired space temperature for human comfort, according to the ASHRAE Standard 55 – 2010. The heat transfer coefficients for the indoor walls and floor surfaces were taken to be 8 W/(m^{2}K) (Shinoda et al., 2019), according to the values provided in existing standards and guidelines (e.g., REHVA, EN1264-5 and ISO 11855-2).

2.2.2 Governing equations and input parameters

In COMSOL, the heat transfer process in all the soil layers was mainly through conduction and can be modelled by considering the energy conservation equation, as follows:

$$\left(\rho C_{\rho}\right)_{eff,s}\frac{\partial T_s}{\partial t}=\frac{\partial}{\partial x}\left(k_{eff,s}\frac{\partial T_s}{\partial x}\right)+\frac{\partial}{\partial y}\left(k_{eff,s}\frac{\partial T_s}{\partial y}\right)+\frac{\partial}{\partial z}\left(k_{eff,s}\frac{\partial T_s}{\partial z}\right) \quad (1)$$

where x, y and z are the spatial coordinates of the entire modelling domain; T_s is the soil temperature (°C) and t is the elapsed time; ρ is the density of saturated soil (kg/m^3); C_{ρ} is the specific heat capacity (J/(kg K)), collectively referring $(\rho C_{\rho})_{eff,s}$ to be the effective volumetric heat capacity of the soil; and $k_{eff,s}$ is the effective thermal conductivity of soil (W/(m K)) (Jayachandran & Reddy, 2019), which can be expressed, as follows:

$$\left(\rho C_{\rho}\right)_{eff,s}=\theta_s\rho_s C_s+(1-\theta_s)\rho_p C_p \quad (2)$$

$$k_{eff,s}=k_s^{\theta_s}\times k_p{}^{(1-\theta_s)} \quad (3)$$

where θ_s is the volume fraction of soil particles; C_s and ρ_s are the specific heat capacity (J/(kg K)) and density (kg/m^3) of dry soil, respectively; C_p and ρ_p are the specific heat capacity and density of pore water, respectively.

Similarly, the heat transfer process in the structural components, including the walls and floor slabs, was mainly through conduction. The energy conservation equation for the wall, for instance, can be expressed as:

$$\rho_w C_w\frac{\partial T_w}{\partial t}=\frac{\partial}{\partial x}\left(k_w\frac{\partial T_w}{\partial x}\right)+\frac{\partial}{\partial y}\left(k_w\frac{\partial T_w}{\partial y}\right)+\frac{\partial}{\partial z}\left(k_w\frac{\partial T_w}{\partial z}\right) \quad (4)$$

where ρ_w, C_w and k_w are the density (kg/m^3), specific heat capacity (J/(kg K)) and thermal conductivity (W/(m K)) of the wall, respectively. The same governing equation applies to the slab. The material properties of the RC slabs were considered to be the same as the RC wall panels.

To model the heat transfer process by the U-shaped heat exchange pipes, nonisothermal pipe water flow was used to simultaneously simulate the variations in flow, pressure, and temperature. The corresponding energy conservation equation can be expressed as follows:

Proceedings DOI: 10.21467/proceedings.171
ISBN: 978-81-970666-7-2

Series: AIJR Proceedings
ISSN: 2582-3922

$$\rho_p A_p C_p \frac{\partial T}{\partial t} + \rho_p A_p C_p u e_t \cdot \nabla_t^{T^2} = \nabla_t \cdot \left(A_p k_p \nabla_t T\right) + \frac{1}{2} f_D \frac{\rho_p A_p}{d_h} |u|u^2 + Q_p + Q_{wall} \quad (5)$$

where A_p is the cross-section area of the pipe (m^2) available for flow; T is the fluid temperature in the U-shaped pipe (˚C), u is the fluid velocity (m/s); k_p is the thermal conductivity of the pipe material (W/(m K)), which is made of high-density polyvinyl chloride in this study. The second term on the right-hand side of the equation represents the friction heat dissipated due to viscous shear, where f_D is the friction factor; d_h is the hydraulic diameter (m); and Q_p is the heat generation (heat source) in the fluid (W); and Q_{wall} is the power loss through the pipe wall (W/m), expressed as follows:

$$Q_{wall} = (hZ)_{eff}(T_{ext} - T)\nabla \cdot \left(\rho_p v\right) \quad (6)$$

where h is the heat transfer coefficient (W/m^2K); Z is the pipe wall perimeter (m); T_{ext} is the external temperature outside the pipe (°C), which is the soil-wall interface temperature obtained from the heat conduction; v is the kinematic viscosity of fluid (m^2/s); and $(hZ)_{eff}$ is the effective heat transfer coefficient, as follows:

$$(hZ)_{eff} = \frac{2\pi}{\frac{1}{r_0 h_{int}} \sum_{n=1}^{N} \left(\frac{ln\left(\frac{r_n}{r_{n-1}}\right)}{\lambda_n}\right)} + \nabla \cdot \left(\rho_p v\right) \quad (7)$$

where r_n is the outer radius of the U-shaped pipe wall (m); and h_{int} is the internal film resistance (W/mK).

Tables 1, 2 and 3 summarise the input parameters of the soil, heat exchange pipe and the RC wall and floor slabs required for the thermal analysis, after Cui et al. (2023), Cui & Zhou (2022) and Ng et al. (2014).

Table1: Summary of the properties of different soil types used in the thermal analysis

Property	Fill	MD	CDG	MDG
Porosity	0.45	0.45	0.38	0.37
Thermal conductivity of solid phase (k_s) (W/ (m· K))	3.26	2.0	3.26	3.26
Saturated soil density (ρ) (kg/m^3)	1937	1937	1937	2243
Heat capacity at constant pressure (C_s) (J/(kg·K))	2239	1200	1500	1500

Table 2: Summary of the input parameters of the heat exchange pipes

Pipe tubes	Value
Thermal conductivity (k_p) (W/ (m· K))	0.42
Inner diameter (mm)	25
Pipe thickness (mm)	5
Distance between the inlet and outlet (m)	1

Table 3: Summary of the input parameters of RC walls and floor slabs

Concrete	Value
Thermal conductivity (W/(m·K))	1.5
Density (kg/m^3)	2400
Specific heat capacity (J/Kg·K)	880
Wall Depth (m)	50
Wall Length (m)	107
Wall Width (m)	1.2

2.2.3 Analysis plan

A series of parametric thermal analyses were carried out to investigate the heat exchange process and efficiency of the energy wall (Table 4). A primary factor that has been recognised to affect the efficiency is the inlet fluid temperature (T_{in}) in the heat exchange pipe. According to a practical reference geothermal heat pump system in Bangkok, Thailand (Takashima et al., 2011), T_{in} typically varies from 35 to 39 °C in tropical climate. In this study, the values of T_{in} of 37 and 40 °C were considered. The initial soil temperature (T_s) and basement temperature (T_B) also play significant roles in the heat transfer process because they directly affect the thermal gradient between the energy geostructure and the surrounding soil. Although an average T_s of 22 °C were reported by Cui et al. (2008), on some occasions the average T_s could vary up to 26.6 °C spatially across Hong Kong (Chow et al., 2011). Thus, warmer ground conditions, say T_s of 24 and 26 °C, were considered, representing worser or more conservative scenarios in terms of heat exchange efficiency. The basement would sometimes be used as a car park. According to survey data collected from an investigation of 22 car parks in

Hong Kong, T_B ranges from 24 to 33 ºC (Chan et al., 1998). Therefore, different values of T_B of 24, 30 and 33 ºC were used to study its impact on the thermal performance of the system. Another variable was the number of wall panels being thermally activated. As depicted in Fig. 2, the long side of the excavation area was retained by 50 wall panels. Three cases were modelled, (1) one energy wall panel (1U; located at the middle of the 50 wall panels); (2) 20 wall panels (20U; located every alternative wall panel) and (3) 50 wall panels (50U).

In all the analyses, the so-called continuous operation mode of the GSHP was simulated; under this mode, the energy wall panels operate for 24 hr a day and without stopping for 25 years. This mode of operation means that the heat was continuously injected to the ground throughout all years and the thermal gradient between the energy wall and the surrounding soil would be reduced as the ground was continuously warmed up, representing a worst-case scenario in terms of heat transfer efficiency. A more realistic GSHP operation mode was also considered, known as intermittent operation; under this mode, the energy wall panels operated for 10 hr in one day, i.e. the normal working hours of an office in each day followed by a 14-hour break in a day. Instead of considering 25 years, the simulation of the intermittent mode was limited to about 200 days, due to the significant constraint of computational power required. The 200-day simulation took 13 days of calculation time; as will be shown later, the simulation results up to this duration were adequate to support the conclusion drawn.

Table 4: Parametric analysis plan

Analysis ID	Inlet fluid temperature T_{in} (˚C)	Initial soil temperature T_s (˚C)	Basement temperature T_B (˚C)	No. wall panel activated (N)
$T_{in37\text{-}1u}$	37	22	24	1
$T_{in37\text{-}20u}$				20
$T_{in37\text{-}50u}$				50
$T_{in40\text{-}1u}$	40			1
$T_{in40\text{-}20u}$				20
$T_{in40\text{-}50u}$				50
$T_{in40\text{-}int}$				1
T_{s26}		26		50
T_{s24}		24		
T_{B30}		22	30	
T_{B33}			33	

*All cases considered continuous operation, except the case $T_{in40\text{-}int}$ which considered intermittent operation. N denotes the number wall panels being thermally activated and used as the energy wall panels.

The key simulation output was the outlet fluid temperature (T_{out}). Based on this output, the heat exchange rate ($q(t)$ as a function of time t) that was normalised by the surface area of wall panel(s) ($A_{w,s}$) can be determined, as follows:

$$q(t) = mC_p[T_{in}(t) - T_{out}(t)]/A_{w,s} \quad (8)$$

where m is the water mass flow rate (kg^3/s). The value of T_{out} can be used to determine the COP (dimensionless) of the GSHP, considering the heating and cooling loads of a simulated building. For energy geostructures that adopted a U-shaped loop arrangement, previous studies found an empirically linear correlation between COP and T_{out} (Kahraman & Celebi, 2009; Casasso & Sethi, 2014), as follows (Jia et al., 2024):

$$COP_{cooling-GSHP} = -0.12T_{outlet} + 8.6 \quad (9)$$

Based on the calculated COP, the cumulative energy consumption (W) can be determined as long as the cooling load ($Q_{cooling}$) of the infrastructure that an energy geostructure is supporting is known:

$$W = \sum_{1^{st}day}^{25^{th}year} \frac{Q_{cooling}}{COP} \quad (10)$$

Unfortunately, $Q_{cooling}$ is unavailable for the Dragon Centre because of a lack of building parameters. In this study, the calculated $Q_{cooling}$ reported by Fong (1999) for a commercial building (with a total floor area of 26,340

Proceedings DOI: 10.21467/proceedings.171
ISBN: 978-81-970666-7-2

Series: AIJR Proceedings
ISSN: 2582-3922

m^2) in Hong Kong was adopted, based on the Typical Meteorological Year (TMY) weather data of Hong Kong. The commercial building envelope consists of a glass curtain wall resembling the Dragon Centre case and was equipped with a central air-conditioning system.

2.3 Thermomechanical soil–structure analysis

The FE package, PLAXIS 2D Thermal (V20), was used to simulate the thermomechanical behaviour of the energy wall from the excavation stage to the subsequent operation stage of GSHP. A plane-strain analysis was conducted, considering all wall panels to be thermally activated (i.e. 50U case). This consideration represents the worst-case scenario in terms of wall structural responses. Detailed model setup, boundary and initial conditions, governing equations, input parameters and analysis plan are explained in the following sections.

2.3.1 Model setup, initial conditions and boundary conditions

Figure 2(b) shows the cross-section view of the deep excavation problem. Similarly, only half of the excavation was modelled, totaling 986 15-node triangular elements. Drained, effective stress analysis was carried out (i.e. no mechanical or thermal consolidation (and their induced excess pore-water pressure) was considered, which is deemed reasonable for modelling sandy materials). According to Lui & Yau (1995), the initial groundwater table was located 1.5 m below the ground surface, establishing a hydrostatic pore-water pressure distribution. Whilst the elevation of the groundwater table on the retained side remained unchanged, the groundwater table was lowered to the ground level after each stage of excavation. The initial soil stress was established under K_0 condition, estimated based on the Jaky's equation. For the mechanical boundary conditions, the ground surface was free to move, whilst the bottom boundary was fixed in both horizontal and vertical directions. No horizontal displacement was allowed on the two side boundaries. Water was allowed to flow out of the two side boundaries with a constant pressure as the hydraulic boundary conditions, whilst no water flow was allowed at other boundaries. For the thermal boundary condition, all side boundaries were set to a constant temperature of 22 ˚C, whilst the soil–wall interface was set to a thermal function to simulate the GSHP operation (see details in Section 2.3.3 below).

2.3.2 Constitutive models and input parameters

The hardening soil small (HSS) model was used to model the mechanical behaviours of the fill and CDG. The Hardening Soil Model (HS) (Schanz et al., 1999) is an elastoplastic model that introduces a yield cap that expands the yield surface upon plastic straining, incorporating a multi-surface yield criterion. The formation of irreversible plastic strains characterises compression and shear hardenings as a result of primary compression and deviatoric loadings. This model has been extended to be capable of capturing the nonlinear strain-dependency of shear modulus (Atkinson, 1990), including the behaviour at the very-small-strain and small-strain ranges, which have been demonstrated to be vital for modelling deep excavation problems. To consider the stiffness nonlinearity, the following hyperbolic equation has been adopted by the HSS model to allow the secant shear modulus G_s to decrease with shear strain (γ) nonlinearly (Santos & Correia, 2001):

$$\frac{G_S}{G_{\max\,(ref)}} = \frac{1}{1+a\left|\frac{\gamma}{\gamma_{0.7}}\right|} \tag{11}$$

where $G_{max(ref)}$ is the reference maximum shear modulus at the very-small-strain at a reference effective minor principal stress, σ'_3; $\gamma_{0.7}$ is the shear strain at which the G_{sec} reduces to 72% of the $G_{max(ref)}$; and a is a fitting parameter, which was typically taken as 0.385 (Santos & Correia (2001)). Due to the lack of experimental data on the stiffness reduction curve for MD, the perfectly-elastic, perfectly-plastic Mohr-Coulomb (MC) model was adopted to describe its mechanical behaviour. The MDG was modelled to behave elastically. All the key input parameters for each type of soil used in the simulation are summarised in Table 4, after Ng et al. (2014).

All soil types were considered to be thermoelastic, meaning that thermally induced changes in soil volume were linearly related to temperature change through the coefficient of thermal expansion (CTE). As most of the soil conditions are sandy and quartz-based materials, the CTE of all the soils was taken be 10με/°C (Agar, 1984).

For the structures, the wall was modelled as a plate element; in this case, the wall was considered to have a unit width and behaved as an elastic beam, which allowed both axial deformation and in-plane bending. The

wall was considered 'wished-in-place', meaning that any wall installation effects were ignored. Each of the five RC slabs was modelled as a fixed-end anchor. No heat transfer was permitted from the wall to slabs. Notably, the area reduction due to the presence of the U-shaped loop in each wall panel was 1.5×10^{-5}%; the associated reduction in the wall moment capacity can be neglected. All the input parameters are summarised in Table 5.

Table 4: Summary of the input parameters required for the three different constitutive models (after Ng et al. 2014)

Soil	γ_{sat} (kN/m^3)	E(MPa)	E_{50}^{ref} (MPa)	m	$\gamma_{0.7}$	G_{max}^{ref} (MPa)	p^{ref} (MPa)	V'	C'(kPa)	φ'_{cs} (˚)
Fill	19	-	25	0.5	1.2E-3	105	27	0.17	0.1	32
MD	19	13						0.17	0.1	32
CDG	19	-	40	0.5	1.6E-3	98	30	0.17	0.1	35
MDG	22	15000						0.2	-	-

* γ_{sat} denotes the saturated unit weight; E_{50}^{ref} denotes the secant Young's modulus at 50% strength at a reference confining pressure p^{ref} ; and m is a power parameter that determines stress-dependent stiffness.

Table 5. Summary of input parameters to model the thermomechanical behaviours of the diaphragm wall and slabs

Components	Wall properties		Slab properties	Thermal property
	E_wI_w (kN/m^2/m)	E_wA_w (kN/m/m)	EsA_s (kN/m/m)	CTE ($\mu\varepsilon/K$)
Diaphragm wall	4,032,000	33,600,000	-	12
Basement G/F	N/A		293,800	
Basement 1/F				
Basement 2/F				
Basement 3/F			261,200	
Basement 4/F				

Note: The value of CTE of the structural components were obtained from Cui & Zhou (2022). *EI* and *EA* is the flexural stiffness and axial stiffness, respectively, where *E* is the Young's modulus; *A* is the cross-sectional area; and *I* is the moment of inertia of the cross-section. The subscript of the symbols *E* and *A*, *w* and *s*, refers to the wall and slab, respectively.

2.3.3 Modelling procedures

The modelling included two phases, namely construction phase and GSHP operation phase. The construction phase modelled the staged excavation, following the construction sequence reported by Lui & Yau (1995). When all the slabs were installed and the excavation reached the final depth, the modelling of the operation phase was commenced by applying the temporal variation of the average wall surface temperature obtained from COMSOL after considering heat transfer from the U-shaped loop to the RC (Fig. 3). It can be seen from the figure that under the continuous operation mode, the wall surface temperature in the case of T_{in} = 40 ºC was the highest, implying potentially a more significant influence on the wall structural responses. Notably, although this modelling approach (i.e. using an output from the thermal analysis as an input of the mechanical analysis) is a simplified way of modelling thermomechanical soil–structure interaction, it has been extensively employed when analysing energy geostructures in previous studies (e.g. Gawecka et al., 2021; Liu & Zhou, 2022, 2023).

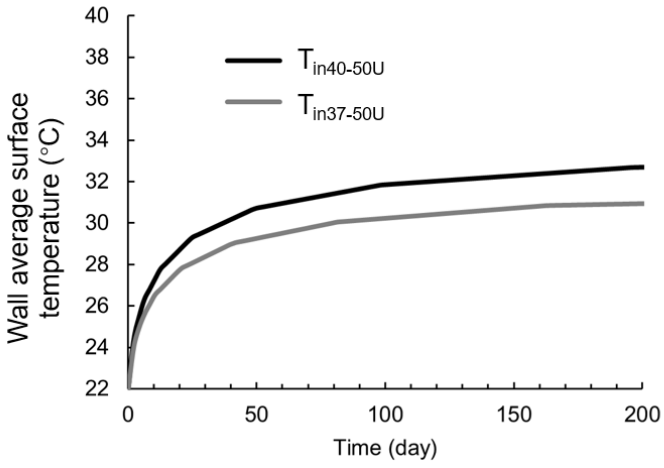

Figure 3: Temporal variations of the average temperature of wall surface output from COMSOL

Proceedings DOI: 10.21467/proceedings.171
ISBN: 978-81-970666-7-2

Series: AIJR Proceedings
ISSN: 2582-3922

3. Results and discussion

3.1 Wall behaviour during the construction phase

Figure 4 shows the computed vertical profiles of wall lateral deflection and wall bending moment obtained from PLAXIS. The computed result at the end of the excavation has a reasonable match with the measured results obtained by an inclinometer, validating the effectiveness of the numerical model. The peak wall displacement was 85.7 mm at 16.2 m depth, 10.8 m above the final excavation depth. The maximum normalised wall movement (i.e. y/H_f, where y is the maximum wall lateral displacement; and H_f is the final excavation depth) in this case was 0.0032 (or 0.32%), which is close to the mean value (i.e. 0.23%) for deep excavation works in Hong Kong that have geological conditions similar to this case study (Ng et al. 2014).

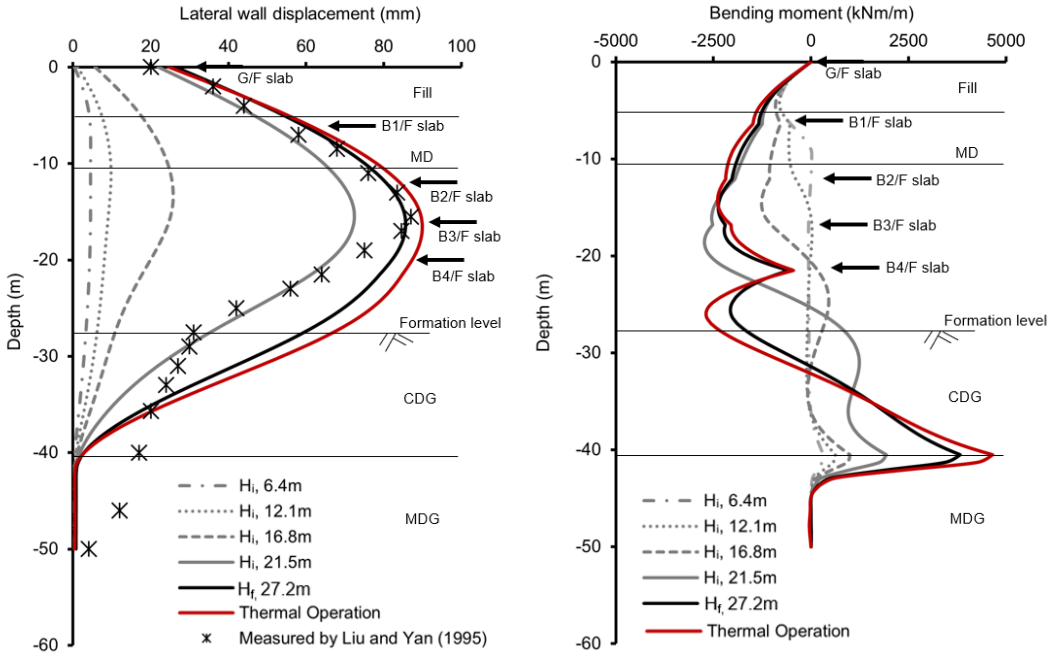

(a) (b)

Figure 4: Vertical profiles of (a) lateral wall displacement; and (b) bending moment subjected to multi-stage excavation and post-excavation thermal operation of 25 years continuous heat injection to the ground. Note H_i denotes the intermediate excavation depth.

Unfortunately, field data on wall bending moment is not available from Lui & Yau (1995), and no direct comparison can be made with the simulation results. Nonetheless, the computed profiles of wall bending moment resembled the shapes typically found in multi-propped excavation. The peak bending moment was 3,822 kNm at a depth of approximately 40.5 m, 13.5 m below the final excavation depth (Fig. 4(b)).

3.2 Operation phase

3.2.1 Variations of soil temperature and outlet fluid temperature

Figure 5(a) shows the computed soil temperature contour at the mid-section of the long-side of the excavation area after 25 years of continuous injection to the ground with T_{in} of 40 °C when all 50 wall panels were thermally activated (i.e. case $T_{in40\text{-}50U}$, again representing the worst-case scenario in terms of heat exchange efficiency). Evidently, the temperature influence zone is approximately 40 m (i.e. 33.D, where D is the wall width) away from the wall. Figure 5(b) shows the temporal variation of soil temperature of six selected monitoring points. These points were at either 50 m (at the wall toe) or 43 m depth (where the temperature increase was the greatest); in each depth, the points that were 0.5D, 1D, and 2D away from the wall were chosen. The continual injection of heat to the ground (i.e. continuous space cooling) led to an exponential increase in soil temperature at all

points, especially for those closer to the wall. After 25 years of continuous operation, a steady state has not been reached and the overall increase in soil temperature from the initial T_s of 22 ºC varied from 12.5 to 15.3 ºC.

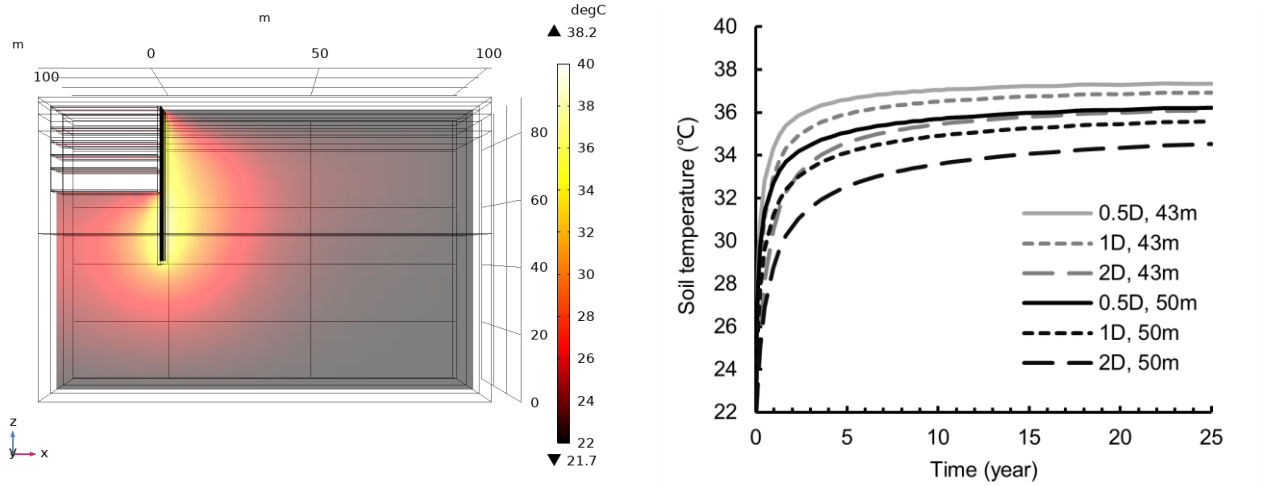

(a) (b)

Figure 5: (a) Soil temperature contour at the mid-section of the long-side of the excavation area after 25 years of operation; and (b) temporary variation in soil temperature at six selected monitoring points around the excavation area under 25 year-continuous operation mode at T_{in} of 40 ºC.

Figure 6(a) shows the temporary variation of T_{out} over about 200 days when considering different T_{in} and the number of energy wall panels. Under the continuous operation mode, exponential increases in T_{out} were identified, following a similar trend of the soil temperature (Fig. 5(b)). At T_{in} of either 37 or 40 ºC, the T_{out} was always higher for greater number of energy wall panels. When only one wall panel (1U) was activated, the heat injected to the ground can be dissipated to not only right behind that energy wall panel but also sideways. As the number of energy wall panels increased, the sideway heat dissipation path became less or even none for the case of 50U. This phenomenon explains the greater increase in soil temperature due to the energy accumulation in the system (Fig. 5(a)) and hence the increase in T_{out} with the number of energy wall panels. After 25 years of operation, the T_{out} approached a steady state value, varying from 34.8 to 37.8 ºC. Accordingly, the normalised heat exchange rate ($q(t)$; Eq. (8)) converged to the range of 10.4 to 12.9 W/m^2. The initial T_s and T_B did play some role in T_{out} (Fig. 6(b)) when considering 50 energy wall panels, yet mainly during the initial stage of operation, and the T_{out} became practically the same after 200 days of operation. The results show that a 9 ºC variation of T_B (i.e. between 24 and 33 ºC) translated to only a 1.2 ºC difference in T_{out} over a period of 200 days.

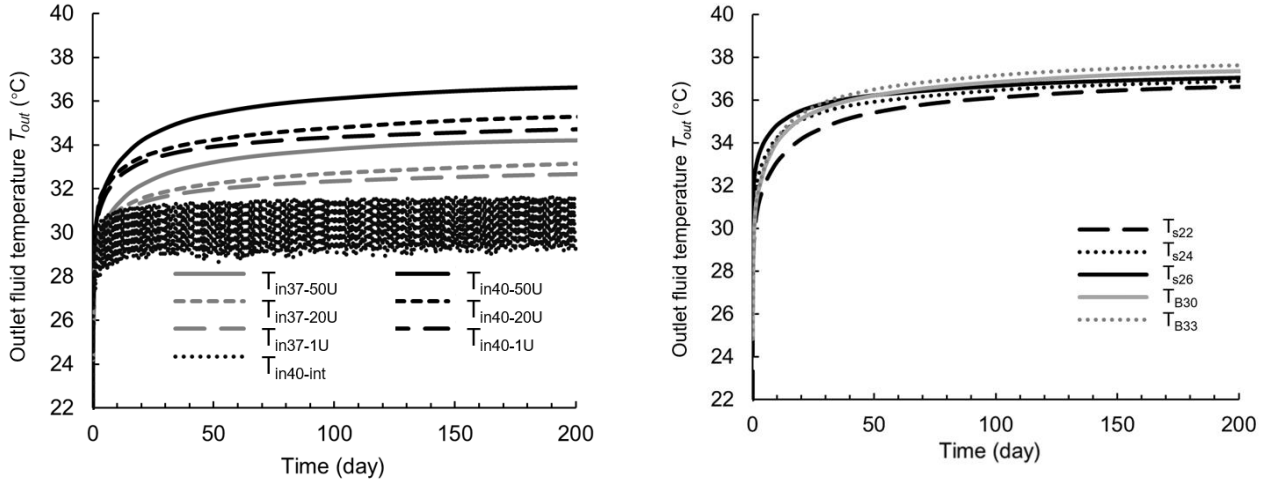

(a) (b)

Figure 6: Temporary variation of T_{out} over approximately 200 days considering (a) different T_{in}, number of energy wall panels and GSHP operation mode when considering the same T_s of 22 ºC; and (b) different T_s and T_B when considering 50 energy wall panels.

Proceedings DOI: 10.21467/proceedings.171
ISBN: 978-81-970666-7-2

Series: AIJR Proceedings
ISSN: 2582-3922

Figure 6(a) also shows the temporary variation of T_{out} under the intermittent operation mode when T_{in} was set to as 40 °C (i.e. case $T_{in40\text{-}int}$). As expected, the T_{out} displayed a fluctuation of approximately 1.5 °C each day due to the nature of the intermittent operation. Importantly, even the upper bound of the T_{out} was significantly lower than that in the case of $T_{in40\text{-}1U}$. The much lower values of T_{out} translated to a greater range of $q(t)$ from 40.8 to 51.7 W/m^2, meaning a much-improved heat exchange efficiency. Indeed, under the intermittent operation mode, the soil-energy wall system allowed 14 hr of heat dissipation and soil temperature recovery every day before the next cycle of 10 hr-operation began. The major discrepancy of T_{out} between the two operation modes highlights the importance of considering a more realistic pattern of the GSHP operation in order to avoid significant overestimation of T_{out} and inappropriate evaluation of the system efficiency in terms of heat exchange.

3.2.3 COP evaluation

Figure 7(a) shows the temporal variation of COP of the GSHP of different cases over approximately 200 days. Initially, a rather high COP of 5.96 can be achieved. However, accompanying the increase in T_{out} (Fig. 6) due to the accumulation of soil temperature (Fig. 5) upon continuous heat injection, the COP of all cases dropped exponentially. Amongst the cases, the drops for the cases with higher T_{in} and a greater number of energy wall panels were the most significant, approaching a stabilised COP between 4.27 and 4.56. Although not substantial, these drops of COP represent the degradation of the efficiency of heat exchange between the energy wall panels and the soil due to the inevitable thermal imbalance problems associated with the high demand of cooling needs under this particular extreme operation mode. However, when considering a more realistic GSHP intermittent operation mode, the drop of COP was much less for a given T_{in} and the number of energy wall panels. The lower-bound COP approached a stablised value of just slightly below 5.00 (i.e. 4.81).

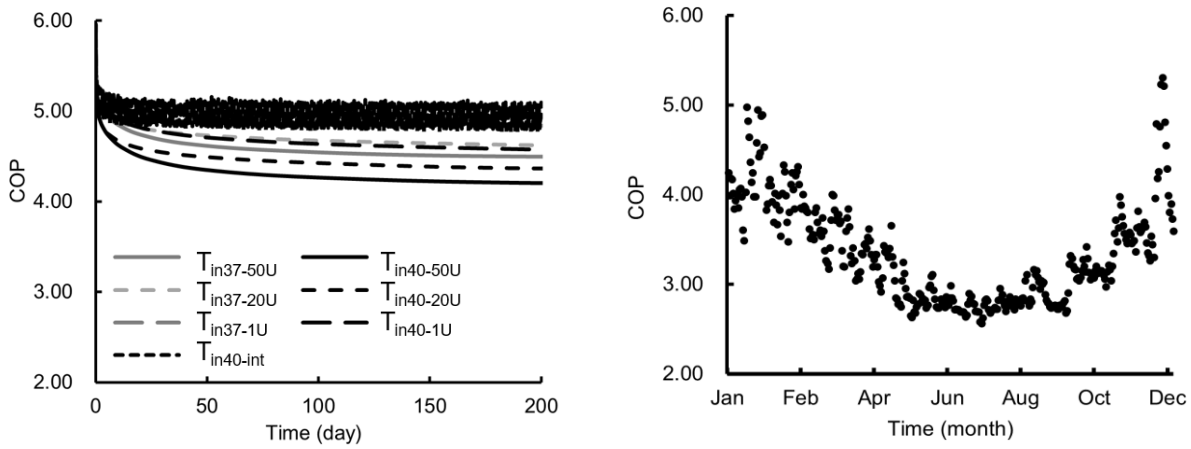

(a) (b)

Figure 7: (a) COP of the GSHP over 100 days; and (b) the daily COP of the ASHP calculated from the TMY data of T_{air}

The COP of the GSHP was compared with that of the air-source heat pump (ASHP), sometimes referred to as an air-cooler chiller, which is typically used in Hong Kong nowadays for cooling purposes. The COP of ASHP can be determined by the following empirical equation (Congedo et al., 2020) that was assumed to be applicable to the environmental condition of Hong Kong's subtropical climate throughout the year (with a mean annual temperature of 22.6 °C), as follows:

$$COP_{ASHP} = -0.00004T_{air}^3 + 0.005T_{air}^2 - 0.2806T_{air} + 7.7483 \quad (12)$$

where T_{air} is the outdoor air temperature of Hong Kong in °C, which was set to be the value obtained from the Typical Meteorological Year (TMY) weather data of Hong Kong (Fong, 1999). As can be seen in Fig. 7(b), the COP varied from 5.31 during winter (heating demand) to 2.63 during summer (cooling demand), and the yearly average COP was 3.34. This comparison highlights that the GSHP system, even considering the worst-case scenarios, can have a much better energy efficiency than the ASHP system.

3.2.4 Energy consumption and carbon emission

Figure 8 shows the monthly $Q_{cooling}$ of the commercial building reported by Fong (1999). Figure 9(a) shows the corresponding cumulative W of the GSHP of three selected cases and the ASHP, all obtained through Eq. (7). The calculation results show that the GSHP, in any case, had much lower W than the ASHP, primarily because the former always displayed a higher COP (Fig. 7). The amount of energy saving, with respect to the case of ASHP, was 30% to 40% under the continuous operation mode and even more than 50% under the intermittent operation mode. The energy saving translated to a reduction in carbon dioxide emission by 13,132 tons, considering that generating 1 kWh of electricity in Hong Kong corresponds to producing 0.55 kg of carbon dioxide in 2022, according to the report from the "CLP Climate-Related Disclosures Report" (CLP 2022).

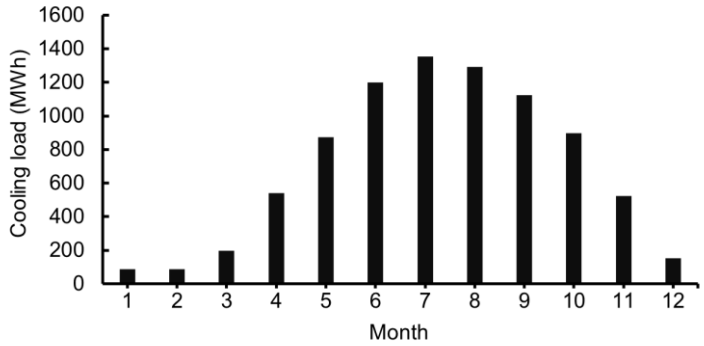

Figure 8: The monthly cooling load of a commercial building in Hong Kong. after Fong (1999).

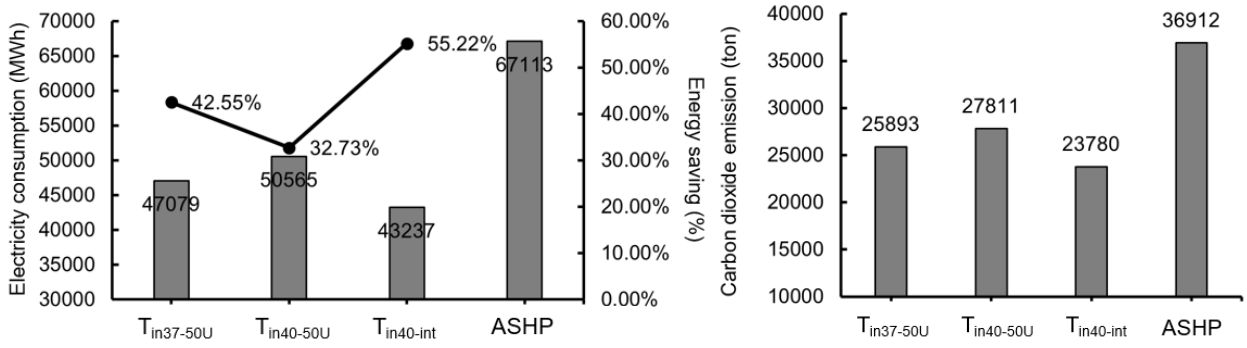

(a) (b)

Figure 9: (a) Cumulative electricity consumption of three selected cases of GSHP and ASHP over 25-year operation; and (b) cumulative carbon emission for the selected commercial building in 25 years

3.2.5 Thermally-induced wall behaviour

Figure 4(a) depicts the vertical profile of the additional wall lateral deflection after 25 years of continuous operation. The thermal expansion of both the energy wall panels and the surrounding soil as their temperature increase due to continuous heat injection caused additional wall movement. Whilst the heating process did not change the shape of the profile much, the wall lateral displacement was magnified, particularly around the depths where the peak was identified. The maximum wall displacement after both the construction and operation phases was 90.0 mm (i.e. 4.3 mm more than the value of 85.7 mm right after the excavation). Correspondingly, the y/H_f rose from 0.0032 during the excavation phase to 0.0033 after the long-term GSHP operation (i.e. less than 5% increased). Notably, the additional outward wall movement under this extreme operation scenario did not introduce any active failure of the soil being retained.

Figure 4(b) shows the profile of wall deflection. Whilst the shape of the bending moment profile was not altered, the maximum bending moment increased from 3,822 kNm after excavation to 4,652 kNm after operation (i.e. 22% increase), accompanying the additional wall movement seen in Fig. 4(a). Because the case study by Lui &

Proceedings DOI: 10.21467/proceedings.171
ISBN: 978-81-970666-7-2

Series: AIJR Proceedings
ISSN: 2582-3922

Yau (1995) did not provide any reinforcement details of the wall panels, the yield bending moment (M_{yield}) needs to be deduced for further interpretation. According to the *Code of Practice for Structural Use of Concrete* 2013 (BD, 2020) and *Structures Design Manual for Highways and Railways* (HyD, 2013), the partial factor for the ultimate limit state design-adjusted structural failure in bending was 1.35. Hence, the M_{yield} was deduced to be 1.35 times the peak bending moment after the staged excavation (i.e. 5,160 kNm). With the known M_{yield}, the thermally-induced increase in the wall bending moment from 3,822 to 4,652 kNm meant a drop of the factor of safety from 1.35 to 1.11. Under these extreme worst-case conditions, additional measures will be needed to take into account the effects of thermal functionality in order to satisfy the specific ultimate limit state design.

CONCLUSIONS

The analyses of the energy and structural performance of GSHP-coupled diaphragm wall demonstrated the high feasibility of adopting this construction technology in Hong Kong, addressing the forthcoming challenges of high energy consumption needs due to air-conditioning to support the government's ambitious strategic spatial development plans. The energy wall used for an underground shopping mall displayed a considerably high COP of up to 5.96 even under extreme energy use scenarios in Hong Kong environment. Although the COP reduced with time due to ground heat accumulation when the heat was continuously injected to the ground, it stabilised at about 4.27, which was higher than the yearly average COP of ASHP (i.e. 3.34) that has been typically used for air-conditioning in Hong Kong nowadays. The amount of COP drop of the GSHP would be much reduced by considering more realistic energy use scenarios such as intermittent operation mode when daily heat injection was not continuous for 24 hr but 10 hr with 14 h-break. The higher COP of the GSHP translated to an energy saving of up to 50% and a reduction in carbon dioxide emission of 35%, when compared to the ASHP. The thermal functionality made the diaphragm wall to experience additional wall lateral displacement and bending moment. The RC wall experienced thermal expansion during continuous heat injection, exerting additional lateral stress and strain to the surrounding soil. Under the extreme 25-year continuous operation mode, the peak wall lateral displacement was increased by less than 5% (i.e. from 85.7 mm after staged excavation to 90.0 mm after thermal operation), yet such increase would not cause any active failure of the retained soil. The increase in the peak bending moment was 22% (i.e. from 3,822 kNm after staged excavation to 4,652 kNm). Although the thermally-induced moment increase did not cause failure against the ultimate limit state, it meant a reduction in the factor of safety (against wall structural failure) from 1.35 to 1.11, and needs of additional measures to account for the effects of thermal functionality of the energy geostructure.

Clearly, validation of the simulation results presented in this study is needed in the future; unfortunately, data concerning the thermal and engineering performance of energy retaining walls is unavailable globally. Ongoing scientific research currently led by the first author focuses on the use of centrifuge modelling technique to study the thermomechanical soil–structure interaction involved in different types of energy geostructures, such as diaphragm walls and tunnels. The new data generated will not only aid the model validation but also provide fundamentals to develop new insights into the design principles of this kind of geostructures due to the additional thermal functionality. The research team is also actively looking for industrial collaboration for any field trials and demonstration of such construction technology to explore the feasibility of adopting energy geostructures in Hong Kong when operating them under the specific environmental conditions in this city.

PUBLISHER'S NOTE
AIJR remains neutral with regard to jurisdictional claims in published maps & institutional affiliations.
HOW TO CITE
Leung *et al.* (2024). Energy Geostructures for Reducing Energy Consumption in Hong Kong: An Example of Energy Diaphragm Wall. AIJR Proceedings, 128-141. https://doi.org/10.21467/proceedings.171.12

REFERENCES

Abuel-Naga, H., Lorenzo, G. A., & Bergado, D. T. 2013. Current state of knowledge on thermal consolidation using prefabricated vertical drains. *Geotechnical Engineering*, 44(4), 132-141.
Agar, J. G. 1984. *Geotechnical behaviour of oil sands at elevated temperatures and pressures* [PhD thesis, University of Alberta].
Atkinson, J. H., Richardson, D., & Stallebrass, S. E. 1990. Effect of recent stress history on the stiffness of overconsolidated soil. *Géotechnique*, 40(4), 531–540.
BD. 2020. *Code of Practice for Structural Use of Concrete 2013 (2020 Edition).* Buildings Department, HKSAR Government, 194 p.
Casasso, A., & Sethi, R. 2014. Efficiency of closed loop geothermal heat pumps: A sensitivity analysis. *Renewable Energy*, 62, 737–746.
Chan, M. Y., Burnett, J., & Chow, W. K. 1998. Energy use for ventilation systems in underground car parks. *Building and Environment*, 33(5), 303–314

Chow, T. T., Long, H., Mok, H. Y., & Li, K. W. 2011. Estimation of soil temperature profile in Hong Kong from climatic variables. *Energy and Buildings*, *43*(12), 3568–3575.

CLP Holdings. 2022. CLP Holdings 2022 Sustainability Report.

Congedo, P. M., Baglivo, C., Bonuso, S., & D'Agostino, D. 2020. Numerical and experimental analysis of the energy performance of an air-source heat pump (ASHP) coupled with a horizontal earth-to-air heat exchanger (EAHX) in different climates. *Geothermics*, 87, 101845-.

Cui, P., Yang, H., Spitler, J. D., & Fang, Z. 2008. Simulation of hybrid ground-coupled heat pump with domestic hot water heating systems using HVACSIM+. *Energy and Buildings*, 40(9), 1731-1736.

Cui, S. Q., and Zhou, C. 2022. Coupled effects of stress state and void ratio on thermal conductivity of saturated soils. *Géotechnique Letters*, 12(2), 148–153.

Cui, S.-q., Zhou, C., Liu, J.-q., and Akinniyi, D. B. 2023. Stress effects on thermal soils and heat transfer efficiency of energy piles in the saturated and unsaturated soils. *Computers and Geotechnics*, 160, 105549.

Fong, S.-K. 1999. BLAST: *Building energy simulation in Hong Kon*g [PhD thesis, Hong Kong Polytechnic University].

Gawecka, K. A., Cui, W., Taborda, D. M. G., Potts, D. M., Zdravković, L., & Loukas, A. 2021. Predictive modelling of thermo-active tunnels in London Clay. *Géotechnique*, 71(8), 735–748.

GEO. 2020. *Guide to Retaining Wall Design (Geoguide 1)* (Continuously updated e-version released on 1 June 2020). Geotechnical Engineering Office, Civil Engineering and Development Department, HKSAR Government, 245 p.

GEO. 2023. *Deep Excavation Design and Construction (2023) (GEO Publication No. 1/2023)*. Geotechnical Engineering Office, Civil Engineering and Development Department, HKSAR Government, 144 p.

Electrical and Mechanical Services Department. 2022. Hong Kong Energy End-use Data 2022 [PDF].

Ground Source Heat Pump Association, 2012. *Thermal pile design, installation and materials standard*s. GSHP Association, UK.

Hsiung, B.-C., & Dao, S.-D. 2014. Evaluation of Constitutive Soil Models for Predicting Movements Caused by a Deep Excavation in Sands. *Electronic Journal of Geotechnical Engineering*, 19.

HyD. 2013. *Structures Design Manual for Highways and Railways (2013 Edition)*. Highways Department, HKSAR Government, 216 p.

Jayachandran, S., & Reddy, K. S. 2019. Estimation of effective thermal conductivity of packed beds incorporating effects of primary and secondary parameters. *Thermal Science and Engineering Progress*, 11, 392–408.

Jia, L., Lu, L., Cui, P., Chen, J., & Pan, A. 2024. A novel study on influence of ground surface boundary conditions on thermal performance of vertical U-shaped ground heat exchanger. *Sustainable Cities and Society*, 100, 105022.

Kahraman, A., & Çelebi, A. 2009. Investigation of the Performance of a Heat Pump Using Waste Water as a Heat Source. *Energies*, 2(3), 697-713.

Liu, J. and Zhou, C. 2022. Thermo-hydro-mechanical behaviour of geothermal energy tunnel in different ground conditions. *Computers and Geotechnics*, 151:104954.

Lui, J., & Yau, P. 1995. The Performance of The Deep Basement For Dragon Centre [PDF].

Ng, C. W. W., Leung, A. K., Kwok, S. S. K., & Yip, F. H. T. 2014. Effects of stiffness nonlinearity on E′ standard penetration test N correlations for analysing wall deflections in Hong Kong excavations. *HKIE Transactions*, 21(1), 35–49.

Santos, J. A., & Correia, A. G. 2001. Reference threshold shear strain of soil: its application to obtain a unique strain-dependent shear modulus curve for soil. *In Proceedings of the 15th International Conference on Soil Mechanics and Geotechnical Engineering (Vol. 1, pp. 267-270)*. Istanbul, Turkey.

Schanz, T., Vermeer, P. A., & Bonnier, P. G. 1999. The hardening soil-model: Formulation and verification. In R. B. J. Brinkgreve, *Beyond 2000 in Computational Geotechnics*, 281.

Shinoda, J., Kazanci, O. B., Tanabe, S.-i., and Olesen, B. W. 2019. A review of the surface heat transfer coefficients of radiant heating and cooling systems. *Building and Environment*, 159:106156.

Takashima, I., Yasukawa, K., Uchida, Y., Yoshioka, M., & Won-In, K. 2011. A geothermal heat pump system in Bangkok, Thailand. I*n Proceedings of the 9th Asian Geothermal Symposium. Ibusuki, Japan, 7–9 November 2011*.

Zhong, Y., Narsilio, G. A., Makasis, N., & Scott, C. 2022. Experimental and numerical studies on an energy piled wall: The effect of thermally activated pile spacing. *Geomechanics for Energy and the Environment*, 100726.